Applied Water Science (2024) 14:267
https://doi.org/10.1007/s13201-024-02322-z

ORIGINAL ARTICLE

Magnetic cork as adsorbent to remove hexavalent chromium from aqueous solution

Juana Abenojar[1,2] · Sara López de Armentia[3] · Juan Carlos. del Real[3] · Miguel Angel Martinez[1]

Received: 18 September 2023 / Accepted: 23 October 2024

Abstract

Chromium contamination of water is a severe environmental problem due to the potential carcinogenicity of Cr(VI). In this work, magnetic cork powder was used as a porous material, and its removal efficiency for Cr(VI) was compared to that of natural cork powder through two mechanisms: adsorption and reduction. Adsorption isotherms and adsorption kinetics were utilized to calculate the reaction rate using a pseudo-first-order model, pseudo-second-order model, and intraparticle diffusion. After adsorption, the powder was characterized by scanning electronic microscopy with energy-dispersive X-ray analysis (EDAX), Fourier transform infrared spectroscopy, X-ray diffraction, and X-ray photoelectron spectroscopy (XPS). EDAX allowed to see a mapping distribution of Fe and Cr, and XPS revealed the presence of Cr_2O_3 and $Cr(OH)_3$, confirming the reduction of Cr(VI) to Cr(III). All the Cr was efficiently reduced and adsorbed onto the surface of the magnetic cork at 20 °C, 27 °C, and 50 °C within 120 min with stirring. The relative efficiencies to the total milligrams of added adsorbent were 98, 98.6, and 99.7 mg, respectively. This is comparable to the adsorption on the natural cork surface at the same temperatures, which measured 97.8, 98.5, and 99.6 mg, respectively, of 100 mg/L Cr(VI) solution. Furthermore, the magnetic cork offers the advantage of being removable by applying a magnetic field.

Keywords Magnetic cork · Industrial waste reuse · Hexavalent chromium adsorption · Ultraviolet–visible spectroscopy

Introduction

The low quality of drinking water causes approximately 80% of diseases and one third of the total death toll in developing countries (Hlavinek et al. 2011). The main cause of this problem is the discharge of insufficiently treated or untreated water. In this scenario, many efforts are made to effectively remove various contaminants from wastewater, such as heavy metals, synthetic colour, sediments, chemicals, radioactive species, pharmaceuticals, and other waste materials (Pesqueira et al. 2020; Guleria et al. 2022; Mohammadi et al. 2022; Miao et al. 2023).

In this research paper, the focus is on heavy metals, which are defined as elements with a density higher than 5 g/cm^3 and include elements such as iron, vanadium, cobalt, copper, manganese, zinc, strontium, and molybdenum. They may be originated from diverse sources, like the combustion of coal, battery manufacturing, and leather industries, to name a few. Heavy metals are the most prevalent pollutant in water and act as poisons to metabolic activities and enzyme inhibitors (Gupta et al. 2021).

One of the most toxic metals that exhibit high stability in water is chromium, especially the hexavalent species (Cr (VI)). It is a toxic metal utilized in various industrial processes, including plating, leather tanning, and pigment production. When released into water sources, it can lead to significant health and environmental consequences. Exposure to hexavalent chromium can cause a range of adverse health effects, such as skin irritation, respiratory difficulties, and cancer. It poses a particular threat to aquatic organisms, as it can interfere with their developmental and reproductive processes (Herrera et al. 2013).

✉ Juana Abenojar
abenojar@ing.uc3m.es

1 Materials Science and Engineering and Chemical Engineering Department/AABI, Universidad Carlos III de Madrid, Av. Universidad, 30, 28911 Leganés, Spain

2 Mechanical Engineering Department/IIT, Universidad Pontificia Comillas, Alberto Aguilera 25, 28015 Madrid, Spain

3 Institute for Research in Technology/Mechanical Engineering Department, Universidad Pontificia Comillas, Alberto Aguilera 25, 28015 Madrid, Spain

Published online: 29 November 2024

There are various analytical techniques used for the determination of heavy metals, focusing on Cr (VI). Atomic absorption spectroscopy offers the advantage of good sensitivity in the determination of metals (1%); however, chemical interference due to different processes derived from atomization leads to a notable alteration in the characteristics of the absorption of the analyte (Pantsar-Kallio and Manninen 1996). For its part, ionic chromatography also allows the analysis of elements of the order of micrograms and generates minimal volumes of waste; however, the saturation of the column due to the presence of organic compounds, oxidizing agents, and chlorides causes changes in the geometry of the retention peaks, leading to false results (American Public Health Association et al. 2012). Colorimetry is considered one of the most straightforward, cheapest, and most efficient procedures due to the excellent accuracy and precision in the quantification of metals present in low concentrations (> 0.1 mg/L) (Herrera et al. 2013). The strategies employed to remove heavy metals from wastewater can be classified as chemical, physical, and biological methods (Cai et al. 2022). Chemical and biological treatment methods involve using chemical agents and microorganisms, respectively, to remove heavy metals from water. Chemical treatments include precipitation, coagulation, and ion exchange (Kerur et al. 2020), while biological include bioremediation and phytoremediation. On the other hand, the most important physical treatment methods are sedimentation, filtration, and adsorption (Kerur et al. 2020). Adsorption involves attaching heavy metal particles (adsorbates) to a solid surface of an adsorbent, such as activated carbon or silica (Karnib et al. 2014). The magnetic cork used in this work can be classified into two different categories proposed by Qasem et al. (Qasem et al. 2021): magnetic adsorbents and bio-adsorbents. Adsorption is a simple, low-cost, and environmentally friendly process as it does not generate harmful by-products, and it has also proved to be an efficient process for many solutes (Spaltro et al. 2018). Besides, the adsorbent used in this work facilitated the reduction of Cr(VI). Therefore, two pathways were followed by adding magnetic cork: adsorption and electrochemical reduction (Qasem et al. 2021).

Cork is a natural material that effectively removes hexavalent chromium from water. The remediation process involving cork includes filling a container with cork and passing the contaminated water through it. The cork acts as a natural adsorbent, attracting and trapping the hexavalent chromium ions in its porous structure, reducing the ions. The trapped chromium can then be safely disposed of, and the purified water can be released into the environment. Previous studies (Sfaksi et al. 2011; Todescato et al. 2021) have shown that cork is a cost-effective and eco-friendly option to remove hexavalent chromium from water. Cork powder is produced during cork processing, where up to 20–30% of the raw material is transformed into cork powders. The annual output exceeds 50,000 t (Wang et al. 2020).

Common adsorbents, such as zeolites (Zanin et al. 2017), activated charcoal (Mohan and Pittman 2006), or synthetic resins (Verma et al. 2023), exhibit high adsorbent efficiency but have certain limitations during the separation process. They are difficult to recover and may cause second contamination. Therefore, one of the challenges in treating wastewater with adsorbents to remove heavy metals is the separation of the adsorbent from the aqueous solution.

To address this limitation, magnetic nanoparticles have gained attention due to their ease of removal by simply applying a magnetic field. Among these, magnetite shows this magnetic characteristic, making it suitable for such applications (Mohamed Khalith et al. 2021). Utilizing magnetite to remove hexavalent chromium involves adding magnetite particles to the contaminated water. The magnetite particles attract and capture the heavy metal ions in their structure through adsorption (Xu et al. 2012). Previous studies have explored the use of magnetic corn stalk (Song et al. 2015), magnetic chitosan resins (Xu et al. 2015), magnetic mesoporous SBA-15 (Wang et al. 2015), and other materials for this purpose.

Combining cork with magnetite could potentially enhance the effectiveness of hexavalent chromium removal from water while also addressing some limitations of each material. Using cork in combination with magnetite could increase the surface area available for hexavalent chromium adsorption, as cork could act as a support material for the magnetite particles. Additionally, cork could help stabilize the magnetite particles, preventing them from settling at the bottom of the treatment system or clumping together. Furthermore, the combination could offer a more sustainable and cost-effective solution for hexavalent chromium removal. Cork is a renewable and biodegradable material that can be sustainably sourced. Besides, the cork powder used in this work is the by waste of the cork industry, making it an environmentally friendly option. Integrating cork and magnetite could lead to an innovative approach to treat wastewater and mitigate the impact of hexavalent chromium contamination. Besides, a wet process to obtain magnetic cork by incorporating magnetite has already been reported in previous works (Abenojar et al. 2020).

Following the adsorption of heavy metals, proper disposal of the utilized adsorbent becomes imperative. The focus on adsorbents loaded with heavy metals arises from their susceptibility to potential secondary contamination, as heavy metal contaminants resist degradation. Inadequate disposal of such used adsorbents can lead to additional environmental pollution. The review conducted by Lata et al. (Lata et al. 2015) compiled data on the removal efficiency and desorption regenerating efficiency of various adsorbents used for heavy metals. In all cases, strong bases and acids were

employed. On the other hand, new strategies involve the use of these adsorbents with the adsorbed heavy metal in catalytic, energy-related, and forensic applications (Velempini et al. 2023).

Conversely, to recover the adsorbent, examples of Cr(VI) removal using biomass were discussed (Gupta and Rastogi 2008), where cyanobacterias were utilized as an adsorbent with an efficiency of 22.9 mg/g. They demonstrated that 80% of chromium could be recovered using 0.1 M HNO_3 and EDTA without causing damage to the adsorption sites. Another study (Sudha Bai and Abraham 2003) investigated fungal biomass as an adsorbent. They used a 0.01N NaOH solution, achieving a desorption efficiency of 78% after 25 cycles. When Na_2CO_3 was used instead of NaOH, the reported efficiency increased to 92%. Maghemite (γ-Fe_2O_4) was employed for Cr(VI) removal (Hu et al. 2005) achieving an impressive efficiency of 95%. Desorption was carried out with a 0.01M NaOH solution, providing an 88% efficiency after six cycles. However, metal-free considerations were not discussed. In another approach (Zelmanov and Semiat 2011), Fe(III) oxide/hydroxide nanoparticles were used as an adsorbent replacing maghemite. Desorption solutions of NaOH and $BaCl_2$ yielded efficiencies of 95–97%, ensuring the complete recovery of the metal. Remarkably, $BaCl_2$ was also obtained for industrial applications in this case.

The most interesting end-of-life strategy for the materials used in this work could be the same proposed in (Ma and Liu 2021). Fe_3O_4/C compounds loaded with Cr(VI) were tested as anodes in potassium-ion batteries. Reversible redox reactions between the hexavalent and trivalent states of chromium generated a continuous flow of electrons throughout the cell, facilitating the movement of K^+ ions.

Hence, this study aims to explore the efficacy of magnetic cork in removing Cr(VI) from water, with a secondary objective of determining the optimal particle size for maximum efficiency. The combination of cork and magnetite presents a promising solution for mitigating water pollution resulting from industrial activities, owing to its affordability, sustainability, and effectiveness. Additionally, the easy recovery of the adsorbent using a magnet enhances its practicality and utility.

Experimental procedure

Materials

Cork particles were supplied by Amorim Cork Composites (Mozelos, Portugal), with two particle sizes: 250–125 µm and 53–38 µm. To produce magnetic cork, it was treated in a low-pressure plasma using the Harrick Plasma Cleaner (Ithaca, NY, USA) with air as the gas to generate plasma at a pressure of 40 Pa. The treatment was carried out for 300 s at 9 W (Abenojar et al. 2014). After the plasma treatment, 2% by weight of the cork was immersed in an aqueous acidic solution (1 L) with a Fe(III): Fe(II) molar ionic ratio of 2:1, as shown in Eq. (1). A basic 2 M ammonium solution (1 L) was then gradually added over the solution. The resulting solution was filtered, and the cork particles with magnetite adsorbed on their surface were washed with deionized water until reaching a pH of 7. The magnetite-loaded cork particles were further subjected to freeze-dried for 12 h using a Telstar LyoQuest freeze-dryer (Telstar, The Netherlands) (Abenojar et al. 2020).

$$Fe^{2+} + 2Fe^{3+} + H_2O \rightarrow Fe_3O_4 + 8H^+ \quad (1)$$

The reagents used in this study were supplied by Sigma-Aldrich (Massachusetts, United States). The reagents included potassium dichromate ReagentPlus® with a purity of ≥ 99.5%; iron (III) chloride hexahydrated ACS reagent with a purity of 97%; iron (II) chloride tetrahydrated for analysis EMSURE®; ammonia solution 25% Suprapur®; and 1,5-Diphenylcarbazide ACS reagent. All the solutions were prepared using deionized water.

Preparation of the solutions

A standard solution of potassium dichromate ($K_2Cr_2O_7$) with a molarity of 4.8×10^{-3} M was used to prepare Cr(VI) (hexavalent chromium) solutions with low concentrations. This solution was prepared by dissolving 141.45 ± 0.02 mg of dichromate in 100 ± 2 mL of deionized water, and the pH lowered to less than 2 by adding 1.5 mL of highly concentrated nitric acid (95% vol.). The accumulated error in the preparation of the original solution was 2.84×10^{-4} mg/mL.

The standard solution contained $0.5 \pm 2 \times 10^{-3}$ mg/mL of Cr(VI). From this solution, a calibration curve was established using an ultraviolet–visible spectrum. Supplementary Table 1 shows the dilutions prepared from aliquots of the standard solution (10, 20, 40. 100, 160, and 200 µL), each made up to 10 ± 0.02 mL with deionized water.

Adsorption procedure

The absorbent capacity of magnetic cork was compared to that of natural cork by preparing Cr(VI) solutions with a concentration of 100 mg/L and 7–8 mg of absorbent in 10 mL of solution. The effect of agitation was examined using an LT-80-PRO Ultrasonic Cleaner 1.5-L ultrasound bath (provided by Tierratech Central, Guarnizo, Spain) operating at a frequency of 37 kHz and 27 °C. Samples were analysed for 15, 60, 120, and 1020 min, with the last one only stirred for 120 min, and compared with unstirred samples at 15 and 1020 min.

The nomenclature used for the samples was "MC" or "C", depending on whether it is magnetic cork (MC) or cork (C), followed by the particle size of the cork. In addition, each sample was numbered with two numbers: the first number corresponds to the type of cork and the second to time and with stirring or not stirring, as seen in Table 1 in results section.

Additionally, a thermodynamic study was conducted by repeating the process for 120 min with stirring at two different temperatures: 20 °C and 50 °C. After adsorption, the cork was filtered, and the magnetic cork was removed using N42 grade nickel-plated disc magnets provided by Supermagnetic (Gottmadingen, Germany).

Once all the dilutions were prepared, 1 mL of a solution containing 50 mg of DF (1.5 diphenyl-carbazide) in 10 mL of acetone was added. DF detects Cr(VI) and turns pinkish depending on the amount of absorbed Cr(VI), at a wavelength of 500 nm. All samples were tested in triplicate and analysed three minutes after the addition of DF. The DF was standardized as an indicator in identifying Cr(VI) in water (Herrera et al. 2013).

The adsorption capacity q_e (mg/mg) was calculated according to Eq. 2. This parameter is used to measure the amount of Cr(VI) adsorbed by the adsorbents. C_i is the initial concentration of Cr(VI) in the solution (100 mg/L), C_e is the equilibrium concentration at a time t (mg/L), V is the solution volume (1 L), and m is mg of adsorbents added (Kooh et al. 2018).

$$q_e(\mathrm{mg/mg}) = \frac{(C_i - C_e)V}{m} \tag{2}$$

Isothermal and kinetics modelling

The adsorption data were analysed using various isothermal models, with the Langmuir (Langmuir 1916) and Freundlich (Freundlich 1906) models being the most employed. The Langmuir model postulates that all active adsorption sites are uniform and that a molecule's ability to bind to the surface is unaffected by neighbouring occupied positions. It further assumes that adsorption occurs only on a monolayer, with no lateral interactions between adsorbate molecules. On the other hand, the Freundlich model posits that the adsorbent is energetically heterogeneous, comprising groups of adsorption sites with characteristic energies. According to this isotherm, there are no lateral interactions between adsorbed molecules, and only a monolayer is adsorbed. The Temkin model was also employed, characterized by considering a uniform distribution of binding energy up to a maximum. It introduces constants whose values depend on the initial adsorption heat and assumes a linear decrease in adsorption heat with the degree of coating (Mahajan et al. 2023). Isotherms were constructed for three concentrations of Cr(VI): 100, 50, and 10 mg/L.

Furthermore, the adsorption kinetics of the metal ion may be impacted by both the adsorption reaction itself and the mass transfer process. To determine the controlling mechanism influencing the rate of Cr(VI) adsorption onto the adsorbent, the following stages are taken into account: (1) the transfer of the metal ion from the solution to the surface of the adsorbent, (2) the actual adsorption of the metal ion onto the adsorbent, and (3) the internal diffusion of the metal ion within the adsorbent. To assess the experimental data, simplified pseudo-first-order (Eq. 3) (Lagergren 1898), pseudo-second-order (Eq. 4) (Ho and Mckay 1999), and intraparticle diffusion (Eq. 5) (Walter et al. 1963), models were applied to Cr(VI).

$$\ln\left(q_e - q_t\right) = \ln q_e - k_1.t \tag{3}$$

$$\frac{t}{q_t} = \frac{1}{q_e^2 k_2} + \frac{t}{q_e} \tag{4}$$

$$q_t = k_3 t^{1/2} + C \tag{5}$$

The Lagergren equation (Eq. 3), known as the pseudo-first-order equation, was the initial rate equation proposed for adsorption in liquid systems. It relies on the solid's capacity,

Table 1 Concentration of adsorbed Cr(VI) per mg of cork $\pm 4 \times 10^{-4}$ mg/mg (q_t)

Conditions	Time (min)		Cr(VI) absorption efficiency (mg adsorbed/mg adsorbent)			
		Initial (mg/L)	MC250/125 (2)	C250/125 (3)	MC53/38 (4)	C53/38 (5)
(1)	0	100				
(2) No stirring	15		5.786	3.456	8.180	7.861
(3) Stirring	15		6.864	4.394	8.050	9.031
(4) Stirring	60		9.025	9.275	10.890	11.833
(5) Stirring	120		11.443	11.059	12.023	11.967
(6) No stirring	1020		13.118	13.020	12.986	13.422
(7) Stirring 120 min	1020		11.291	10.838	13.447	13.495

with k_1 representing the pseudo-first-order constant (min^{-1}), and q_e and q_t denoting the adsorption capacities at equilibrium and time t, respectively. The values of k_1 and q_e are determined from the slope and intercept of the linear form of the pseudo-first-order equation, being plot $ln(q_e\text{-}q_t)$ vs t.

The pseudo-second-order model (Eq. 4) posits that the rate-limiting step in an adsorption process is the mass transfer of the metal ion from the solution to the surface of the adsorbent where k_2 (mg mg^{-1} min^{-1}) is the rate constant, being q_e and k_2 obtained from the linear plot of t/q_t vs t.

For the intraparticle diffusion model q_t is plotted versus $t^{1/2}$ to get a straight line (Eq. 5). k_3 ((mg mg^{-1} min^{-1}) is calculated from slope and C is the intercept of the linear form. This model explains the process in three steps: (1) adsorption on the external surface or instantaneous adsorption; (2) gradual adsorption, where intraparticle diffusion is controlled; and (3) final equilibrium step, where the solute moves slowly from the larger pores to the micropores causing a slow adsorption rate.

The best models to describe the adsorption could be determined considering the R^2 from adjustment to the straight line for each model. It can also be determined by others error functions as Chi-square test (χ^2) (Eq. 6) and the sum of absolute error (EABS) (Eq. 7). In both cases, the experimental q_e obtained and that calculated according to the corresponding kinetic model are compared.

$$\chi^2 = \sum_{i=1}^{n} \frac{\left(q_{e,\exp} - q_{e,\mathrm{cal}}\right)^2}{q_{e,\mathrm{esp}}} \tag{6}$$

$$\mathrm{EABS} = \sum_{i=1}^{n} \left|q_{e,\exp} - q_{e,\mathrm{cal}}\right| \tag{7}$$

Thermodynamics experiments

To study the influence of temperature on the adsorption of Cr(VI) ions, experiments were carried out at 20, 27, and 50 °C for 120 min, with 100 mg/L Cr(VI) solution in an ultrasonic bath with water. The thermodynamic study at different temperatures was carried out for all cork types. Following van't Hoff equation (Eq. 10), obtained from Eqs. 8 and 9, Gibbs free energy can be calculated as explained in (Constales et al. 2017a) and (Ahmad and Hasan 2017).

$$\Delta G^0 = -\mathrm{RT}\ln K_c \tag{8}$$

$$\Delta G^0 = \Delta H^0 - T\Delta S^0 \tag{9}$$

$$\ln K_c = -\frac{\Delta H^0}{RT} + \frac{\Delta S^0}{R} \tag{10}$$

$$K_c = \frac{C_i - C_e}{C_e} \tag{11}$$

K_c was calculated according to Eq. 11, being C_i the initial Cr(VI) concentration and C_e the concentration in the liquid phase in the equilibrium reached at 120 min (Kooh et al. 2017). $Ln\ k_c$ vs $1/T$ was plotted to obtain the thermodynamic parameters ΔH and ΔS.

Experimental techniques

- Ultraviolet-visible spectroscopy

  The calibration curve for Cr(VI) concentrations specified in Supplementary Table 1 was obtained using a Cary 4000 UV–Vis spectrometer (Agilent Technologies, Santa Clara, CA) at a wavelength of 500 nm. Distilled water in a 10-mL glass cuvette was used as the blank. Subsequently, approximately 7.5 ± 0.02 mg of different types of cork was added to the samples containing $0.1 \pm 4 \times 10^{-4}$ mg/mL of Cr(VI), and they were stirred in an ultrasonic bath for 15–120 min. Samples were analysed at different time intervals, filtered, and then, the DF indicator was added, leaving three minutes for colour development. Each sample was analysed three times using the same 10-mL glass cuvette.

- Scanning electron microscope

  The cork and magnetic cork particles were studied using scanning electron microscopy (SEM) with EDAX on a Philips X-30 model (Philips Electronic Instruments, Mahwah, NJ, USA) before and after the absorption of Cr(VI).

- X-Ray Diffraction

  X-ray diffraction (XRD) was performed using a Philips PANalytical X'Pert Pro MRD system (Malvern PANalytical Limited, Malvern, UK). Diffractograms were acquired by plotting intensity versus 2θ in the angular range between 10° and 90°, with a step size of 0.02° and a step time of 2.4 s per step. Cu K-α radiation and Ni filter at a generator voltage of 40 kV and a current of 40 mA were used. The presence of magnetite was confirmed by the coincidence of the pattern number of the magnetite (JCPDS No. 89–2355).

- Attenuated total reflectance Fourier transform infrared spectroscopy.

  Infrared spectra were obtained using a Tensor 27 Fourier Transform Infrared (FTIR) spectrometer (Bruker Optik GmBH, Madrid, Spain). The spectra were recorded

using the Golden Gate attenuated total multiple reflection (ATR) device with 42 scans, averaged with a resolution of 4 cm^{-1}, and collected in the range from 400 to 4000 cm^{-1}. In this study, ATR-FTIR was used to determine the functional groups of cork and magnetic cork particles or/and to assess any variations after Cr(VI) adsorption.

- X-ray photoelectronic spectroscopy

  The surface chemical composition of cork and magnetic cork was analysed using XPS before and after Cr(VI) adsorption. The analysis was conducted using an ellipsoid scan probe with a major diameter of 400 µm, and carbon peak (C–C/C–H) at 284.6 eV was used as the energy calibration standard. XPS spectra were recorded on a Kratos XSAM 800 spectrometer (Kratos Analytical Ltd. Designs, Shimadzu Group Company, Manchester, UK), operating in fixed analyser transmission mode, using Mg Kα (1253.6 eV) excitation. Survey spectra were recorded in the kinetic energy range of 0–1300 eV with 0.5 eV steps. Photoelectron lines of the principal constituent elements, such as O1s, C1s, Cr2p, and Fe2p, were recorded with 0.1 eV steps. Then, deconvolution peaks were fit with a combination of Gaussian and Lorentzian at 50%.

Results

Adsorption study

Supplementary Fig. 1 shows the calibration curve performed. The curve was repeated three times, and no variations were found between the values of absorbance obtained. The calibration curve has the equation $y = 0.0345x$, with $R^2 = 0.9988$. This calibration curve was used to determine the amount of adsorbed Cr(VI) by the cork or magnetic cork added to Cr(VI) solutions with a concentration of 100 mg/L during different time intervals. Both MC and C 250/125, and MC and C 53/38 were used. Magnetic cork has the advantage of being removable without the need for filtration.

According to the World Health Organization (WHO), the standard limit for chromium in drinking water is 30 µg/L (World Health Organization 2017). However, a few years earlier, this limit was 50 µg/L or 100 µg/L according to WHO or The United States Environmental Protection Agency (US EPA) (Wang et al. 2016), respectively. Meanwhile, the standard for drinking water, ISO 18412:2005, covers a range from 2 to 50 µg/L. In this work, a concentration of 5 mg/L of $K_2Cr_2O_7$ was studied, which is equivalent to 0.354 mg/L of Cr(VI) (Yang et al. 2020), or a concentration of 1.600 mg/L (Chen et al. 2018), both falling within the range for residual water according to ISO 11083:1994, which covers concentrations from 0.300 to 0.500 mg/L. The concentrations used in the study are more similar to the highest concentration employed. Higher concentrations were used to account for potential levels found in wastewater of industries such as coatings or leather tanning. The proposed treatment could offer better control of their discharges. The concentration range used represents typical concentrations in Cr(VI) absorption techniques by different methods (Qasem et al. 2021).

Table 1 presents the mg of Cr(VI) adsorbed per mg of adsorbent, which corresponds to q_t (mg/mg). This concentration was calculated from the average absorbance for the mixture, applying the calibration line. Starting from an initial absorbance of 3.44 a.u. (Supplementary Table 2), corresponding to a concentration of 100 mg/L of Cr(VI), the absorbance decreases over time independently of the type of cork used (and Supplementary Table 2 and Supplementary Fig. 2). Consequently, all the solutions reached a concentration of 0.03 mg/L at any time, which corresponds to the standard limit set by the WHO for drinking water (World Health Organization 2017). This means the total milligrams added of MC53/38 and C58/38 adsorbed 99.9 mg of Cr(VI) at 30 °C and 1020 min. At 1020 min, both MC250/125 adsorbed all the Cr(VI) without agitation, but the C250/125 adsorbed 95.6 mg of Cr(VI). However, when stirred for 120 min before resting for 900 min, the larger particles formed agglomerate; thus, the absorbance did not increase after 120 min. The absorbance variation curves at 1020 min are clearly seen in Supplementary Fig. 2, corresponding to condition number 7 (1020 min with stirring 120 min). Samples 7-4 (MC53/38) and 7-5 (C53/38) presented very low absorbance, indicating a very low concentration of Cr(VI), even below the standard limit.

Beakers for 1020 min are shown in Supplementary Fig. 3. Beakers 6-2 (MC250/125) (Supplementary Fig. 3A), 7-4 (MC53/38), 6-5 (C53/38), and 7-5(C53/38) (Supplementary Fig. 3B) showed a clear solution, indicating that the DF indicator did not complex with Cr(VI) because it was all adsorbed by the cork. These samples are highlighted in Supplementary Table 2. This aligns with the values seen in Table 1 Supplementary Fig. 2. However, beakers 6-3 (C250/125), 7–2 (MC250/125), 7–3 (C250/125) (Supplementary Fig. 3A), and 6-4 (MC53/38) (Supplementary Fig. 3B) still appeared pinkish since they contained Cr(VI) in the solution. The most concentrated were beakers 7-2 (MC250/125) and 7-3 (C250/125) (Supplementary Fig. 3A) due to the agglomeration of the cork particles. When the magnetic cork was used, it could be easily removed from the aqueous solution by a magnetic field, as shown in Supplementary Fig. 4 in the right beaker.

The liquid phase adsorption isotherms can be described according to the shape and curvature established by Giles

et al. (Giles et al. 1960). In this case, all four materials followed linear behaviour. This means that the adsorption capacity was proportional to the equilibrium concentration in the liquid phase until the maximum adsorption capacity was reached. Therefore, the active centres remained constant, generated by the high affinity between the adsorbent (cork) and the adsorbate (Cr(VI)). Additionally, the isotherms, according to Hinz et al. (Hinz 2001), belonged to subgroup 1, as they did not show any plateau, indicating no adsorbent saturation.

Adsorption mechanism

As shown in Fig. 1a, the Langmuir isotherm model fits well for the four types of cork, with high R^2 values of 0.9944 and 0.9946. This indicates that all active adsorption sites are uniform, and a molecule's ability to bind to the surface is unaffected by neighbouring occupied positions. Additionally, adsorption occurs only on a monolayer, with no lateral interactions between adsorbate molecules. However, the Freundlich isotherm (Fig. 1b) provides a relatively low R^2 value of 0.9103, similar for all four cork types, although only CM53/38 is represented. In contrast, the Temkin isotherm (Fig. 1b) fits correctly. This suggests a uniform distribution of binding energy and accounts for interactions between the adsorbate and the adsorbed species, as the Temkin isotherm considers these interactions.

For kinetic adsorption studies analysed as a first order reaction, the natural logarithm of concentration of adsorbed chromium in relation to initial concentration ($Ln\ (C_t/C_i)$) versus time is plotted in Fig. 1c (Constales et al. 2017b). The trend for the four curves showed fast adsorption at the beginning of the reaction up to 120 min, followed by a plateau for MC250/125 and C250/125. However, MC53/38 and C53/38 continued adsorbing up to 1020 min, albeit at a slower rate. This could be due to their larger specific surface area, which provides more active centres for MC53/38 and C53/38. From this point, the adsorption process either stopped or continued until all chromium was adsorbed, depending on the particle size. It was found that the first stage of the reaction takes up to 120 min, and it can be considered a straight line. For this reason, the equilibrium time for all reactions is considered to be 120 min. In general, the reactions were quick; most of the Cr(VI) was removed around 2 h with stirring. Other studies have found similar values for pesticide adsorption on carbon materials (Sanz-Santos et al. 2021).

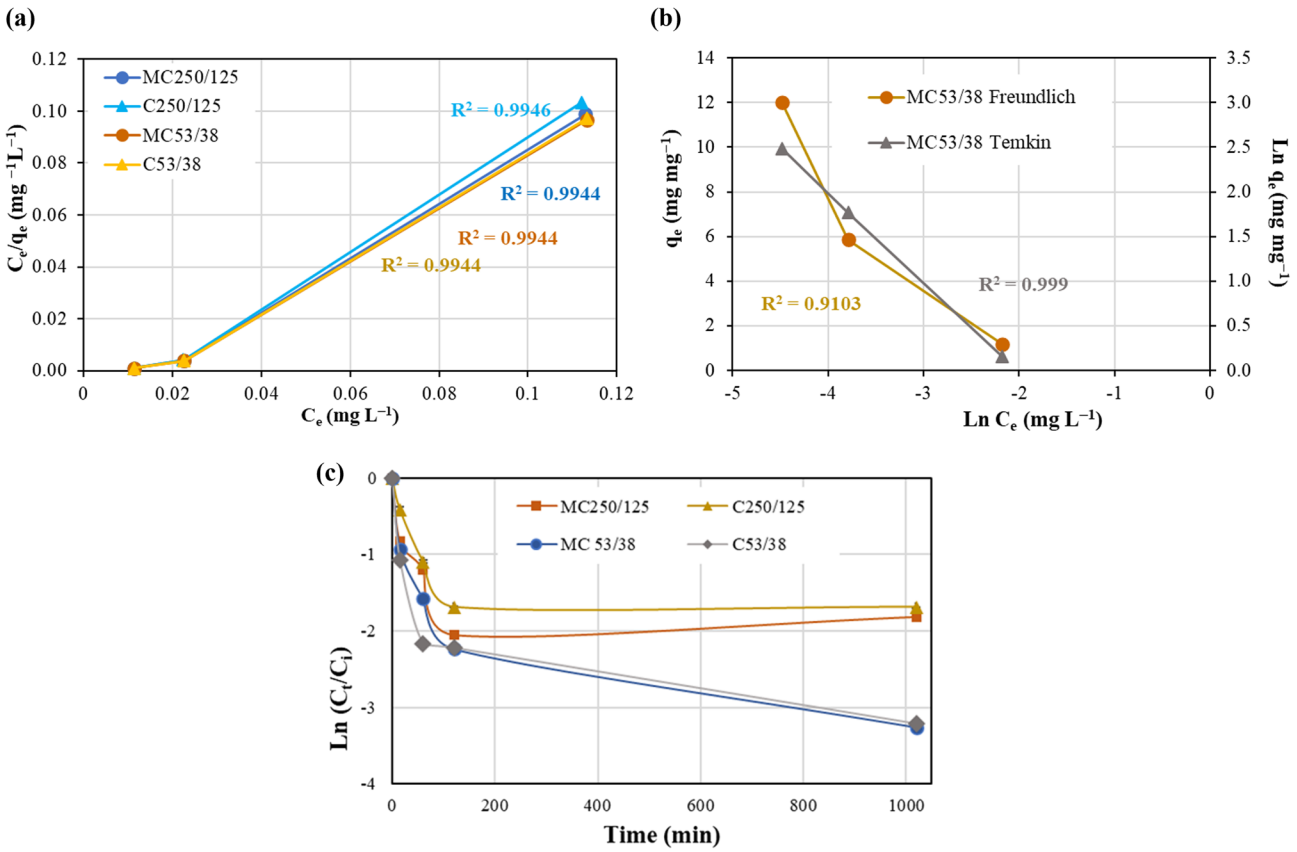

Fig. 1 **a** Linear plots of Langmuir isotherm models for the four types of cork and **b** Freundlich and Temkin isotherm models for MC53/38; **c** adsorption kinetic considering a reaction of first order for the four types of cork

The kinetic models according to Eqs. 3, 4 and 5 were represented and adjusted to a straight line, as seen in Fig. 2. The slopes of the lines and the ordinates at the origin allow the calculation of the equilibrium constants, and the calculated q_e ($q_{e,\,cal}$) will be compared with the experimental q_e ($q_{e,\,exp}$). The relation between $q_{e,\,cal}$ and $q_{e,\,exp}$ provides the error functions χ^2 and EABS according to Eqs. 6 and 7. From Fig. 2, the fits seem more accurate for the pseudo-second order (Fig. 2b), which may be the kinetic model for the adsorption of Cr(VI) with MC and C. Intraparticle diffusion model (Fig. 2c) has worse fits for the four adsorbents, whereas pseudo-first order model (Fig. 2a) has more different fits depending on the cork type.

The kinetic parameters for the adsorbents are shown in Table 2. The R^2 values for MC53/38 and C53/38 were the highest for pseudo-second-order model, although for pseudo-first order model R^2 values were also high. Therefore, both models could be suitable to describe the kinetic data. However, for MC250/125 and C250/125 pseudo-first-order model was more appropriate to define the kinetic adsorption. Pseudo-second-order kinetics imply that the adsorption rate is related to the adsorption sites on the adsorbent surface rather than within the bulk adsorbate. This is related to the specific surface area of the particles, being

Table 2 Parameters from the pseudo-first-order, pseudo-second-order, and intraparticle diffusion kinetic models for the adsorption of Cr(VI) onto cork

Absorbent	MC250/125	C250/125	MC53/38	C/53/38
Pseudo-first order				
q_e, cal (mg/mg)	11.7048	14.2392	7.6316	5.0937
q_e, exp (mg/mg)	11.4433	11.0587	12.0229	11.9669
k_1 (min^{-1})	0.0118	0.0395	0.0354	0.0535
R^2	0.9510	0.9853	0.9901	0.9825
$\chi 2$	0.01	0.91	1.60	3.95
EABS	0.26	3.18	4.39	6.87
R_L	0.46	0.20	0.22	0.16
Pseudo-second order				
q_e, cal (mg/mg)	12.7877	14.0845	12.9534	12.5313
q_e, exp (mg/mg)	11.4433	11.0587	12.0229	11.9669
k_2 (mg mg^{-1} min^{-1})	0.0045	0.0022	0.0077	0.0161
R^2	0.9295	0.9610	0.9994	0.9994
$\chi 2$	0.16	0.83	0.07	0.03
EABS	1.34	3.03	0.93	0.56
Intraparticle diffusion				
k_3 (mg mg^{-1} min^{-1})	0.6437	0.9521	0.567	0.4252
R^2	0.9925	0.9574	0.9647	0.8269
C	4.2673	1.0787	6.0547	7.7445

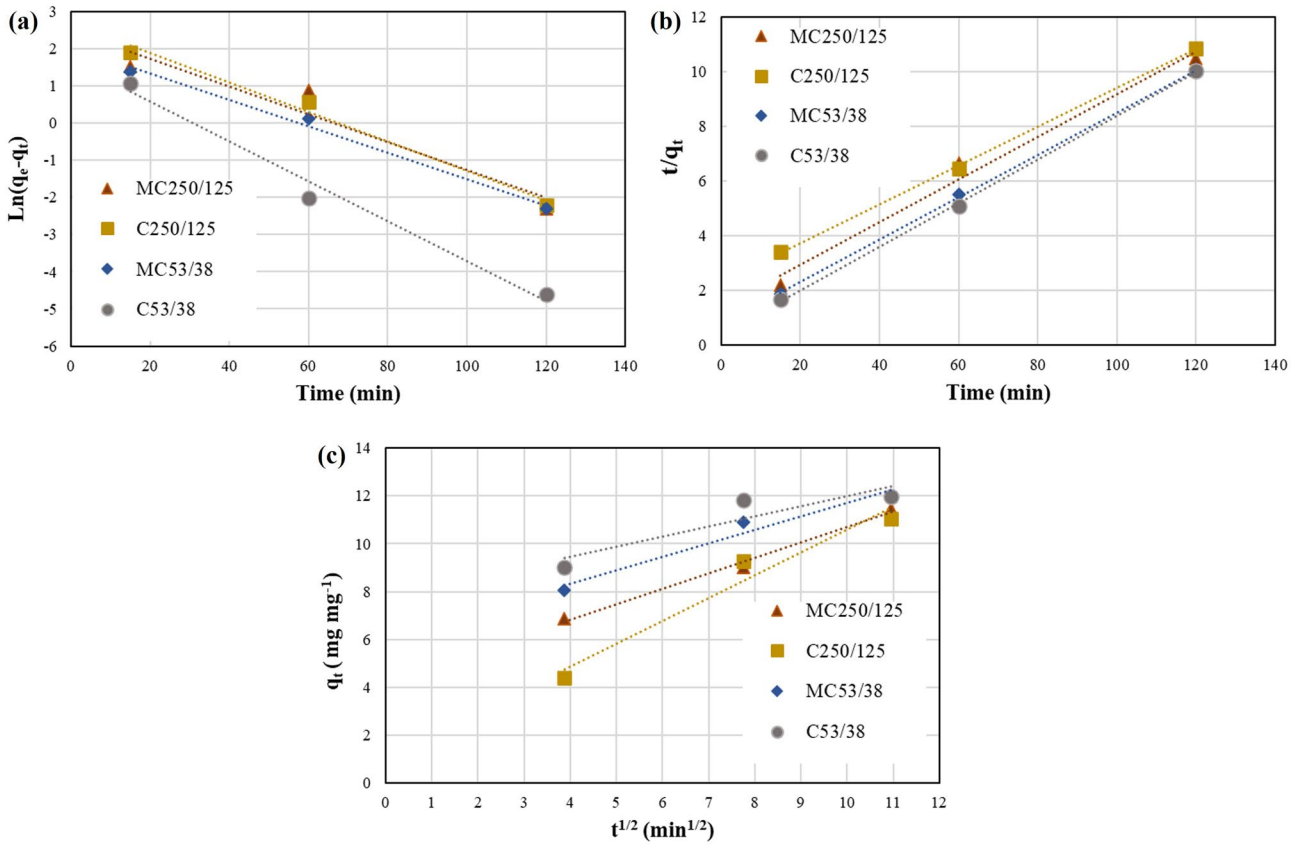

Fig. 2 Linear plot of kinetic models: **a** pseudo-first-order, **b** pseudo-second-order, and **c** intraparticle diffusion

higher for the small particles, as also deduced from Fig. 2. A higher specific surface area results in more active centres for adsorption.

The pseudo-first-order model relies on the solid capacity; thus, it agrees with the Langmuir model. In this case, all active adsorption sites are uniform and the ability of the adsorbate to bind to the surface is unaffected by neighbouring occupied positions. It furthers that adsorption occurs only on a monolayer, with no lateral interactions between adsorbate molecules. The poor fit to pseudo-first order is consistent with the number of available sites, which does not correspond to q_e in the pseudo-first-order model.

The adsorption capacity of MC250/8125 is the least well-fitted to the two previous models, being more consistent with intraparticle diffusion.

Adsorption thermodynamics

To obtain the thermodynamic parameters, ln k_c vs $1/T$ was plotted (Fig. 3), obtaining the values of ΔH from the slope and ΔS from the intercept of the linear form, according to Eqs. 8–11.

The positive value of $\Delta H°$ suggests that adsorption is an endothermic reaction (Table 3). Additionally, the positive value of $\Delta S°$ indicates an increase in randomness at the solid–solute interface during Cr(VI) removal, attributed to the release of water molecules around Cr(VI) due to structural changes occurring in the cork. These structural changes may be induced in the carbonyl and ester groups of the cork surface. ΔG° values confirm that the adsorption of Cr(VI) is thermodynamically feasible and spontaneous. The three variables have higher absolute values in the MC53/38, which coincides with the adsorbent that retains the highest amount of Cr(VI).

Other researchers, such as (Ahmad and Hasan 2017), have also observed endothermic and spontaneous adsorption reactions for Cr(VI) with 2,4-DNP onto XGP@ZnO. In the case

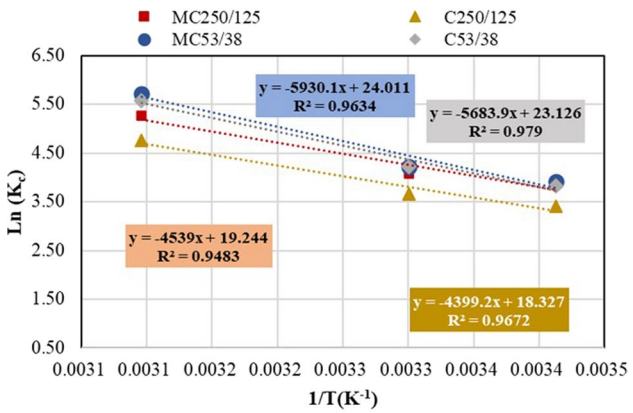

Fig. 3 Calculation of thermodynamic adsorption parameters

Table 3 Thermodynamic adsorption parameters

	Temperature (K)	MC250/125	C250/125	MC53/38	C53/38
ΔH° (kJ/mol)		37.74	36.57	49.30	47.26
ΔS° (kJ/mol K)		0.16	0.15	0.20	0.19
	293	− 9.14	− 8.1	− 9.19	− 9.08
	300	− 10.74	− 9.1	− 10.59	− 10.42
	323	− 13.94	− 12.6	− 15.18	− 14.85

of MC53/38 and C53/38 at 50 °C, more spontaneous adsorption reactions are achieved. This is evident as, according to the Ellingham diagrams, the $\Delta G°$ values are more negative, indicating greater spontaneity in the reactions.

Comparison of adsorption capacity for the removal of Cr(VI)

The adsorption rates are 99% for C53/38 and MC53/38 at 50 °C for 120 min, while they vary from 96 to 93% for MC250/125 and C250/125, respectively. These values are consistent with those reported in the literature, as shown in Table 4. Lower temperatures result in lower adsorption rates, with 87% and 82% for MC250/125 and C250/125, respectively, compared to 90% for MC53/38 and C53/38 at 27 °C. These findings are based on an initial concentration (C_i) of 100 mg/L and a variable amount of adsorbent ranging from 7 to 8 mg.

Characterization of cork and magnetic cork after adsorption

Scanning electronic microscopy

Supplementary Fig. 5 shows the C53/38 and MC53/38, and Fig. 6 corresponds to C250/125 and MC250/125 taken with two different detectors, CBS (circular backscatter) (Supplementary Fig. 5A and C, and Supplementary Fig. 6A and B) and ETP (Everhart Thornley) (Supplementary Fig. 5B and 5D, and Supplementary Fig. 6C). CBS used the All mode, providing an image depending on the Z number. ETP used the SE (secondary electron) mode, and the image was created considering the topographic contrast.

When observing the C (Supplementary Fig. 5A and B, and Supplementary Fig. 6A), the cell morphology of the cork was clearly visible. However, the structure seemed more compact in the MC (Supplementary Fig. 5C and D, and Supplementary Fig. 6C and D). The density increased from 1.6 g/cm^3 (for *C*) to 1.8 or 1.9 g/cm^3 (MC) (Abenojar et al. 2020), but the specific surface area decreased.

Table 4 Comparison of adsorption capacity for the removal of Cr(VI)

Adsorbent	Contaminant	Removal efficiency	Refs
Cork	Chromium	97% eliminated in 3 h	(Sfaksi et al. 2011)
Cork	Chromium	Completely removed in less than 100 h, Cr^{3+} remaining	(Todescato et al. 2021)
Clinoptilolite zeolite	Iron, copper, chromium	85.1% Cr eliminated in 90 min	(Zanin et al. 2017)
Activated carbon	Chromium	90% eliminated in 24 h	(Das et al. 2000)
Dextrin-Fe_3O_4	Chromium	96% eliminated in around 100 min at 50 °C	(Mittal et al. 2016)
Chitosan-grafted polyaniline	Chromium and cadmium	Completely removed in 2 h	(Ahmad et al. 2017)
Magnetite carbon	Chromium	99% of elimination in 5h	(Mohamed Khalith et al. 2021)
Magnetite corn stalk	Chromium	Completely removed in 8 h	(Song et al. 2015)
Magnetite cork	Chromium	Removed 99% at 120 min (50 °C)	This study

Thus, the specific surface of C250/125 and C53/38 was $0.123 \pm 2 \times 10^{-3}$ and $0.239 \pm 3 \times 10^{-3}$ m^2/g, respectively. In contrast, there was a decrement in specific surface area after treatment for the magnetic cork, measuring $0.112 \pm 2 \times 10^{-3}$ m^2/g and $0.237 \pm 3 \times 10^{-3}$ m^2/g, for MC250/125 and MC53/28, respectively. This means that the magnetic cork may have less efficiency as an adsorbent of chromium, especially in the case of particles with greater granulometry.

EDAX analysis for magnetic cork is shown in Figs. 4 and 5. Fe presented 40% before and 38% after the adsorption process. EDAX analysis was carried out in the centre of Fig. 5A. Figure 5B corresponds to the mapping for Fe and Cr, with Fig. 5C and D showing the mapping of the separated elements. The main conclusion is that a homogeneous distribution on the total surface was appreciated.

Although the semiquantitative characteristic of this analysis, the amount of C and O (Fig. 5E) is similar to Fig. 4, and the remaining percentage corresponded to Fe and Cr. As seen previously (Table 1), the maximum adsorbed chromium is 13.495 mg/mg of absorbent; this amount is equivalent to 1 wt% of the cork surface, according to Fig. 5E.

X-ray diffraction

The natural cork is an amorphous material; thus, it presents a broad peak around $2\theta = 20°$ when observed by X-ray Diffraction. Nevertheless, the magnetite on the cork particles could be checked using XRD. The diffractogram peaks correspond to the presence of iron oxides (Supplementary Fig. 7). Fe_3O_4 peaks appear at 2θ values of 30.1°, 35°, 43°, 53°, 56.9°, and 62.5°, which are attributed to planes (220), (311), (400), (422), (511), and (440), respectively (Mohammadkhani et al. 2019). These planes correspond to the cubic crystalline structure of the reverse spinel type, typical of magnetite.

Once the chromium was adsorbed, the diffractogram peaks did not change. Magnetite and the amorphous peak were found. After normalizing the peaks with respect to the iron principal, the only difference found was in the area of the amorphous peak. This may be due to a lack of crystallinity in the adsorbed chromium (Kumar et al. 2020).

Infrared spectroscopy (FTIR-ATR)

In addition to XRD, infrared spectroscopy (FTIR-ATR) was used to determine the functional groups found in the cork and the possible variations after chromium adsorption. Cork and magnetic cork had already been previously analysed (Abenojar et al. 2020).

Bands around 3100–3850 cm^{-1} in all spectra (Fig. 6A and B) could be assigned to the H–O–H stretching and bending vibration modes of the adsorbed or free water. The double peak at 2850–2923 cm^{-1} was associated with the stretching vibration of C–H bonds of CH_3 and CH_2 groups, respectively. From 2600 to 1800 cm^{-1}, there were no peaks. All spectra (Fig. 6A and B) also showed assigned bands to the

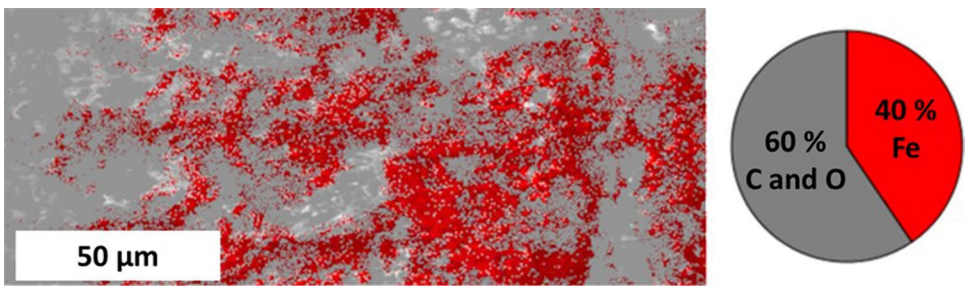

Fig. 4 EDAX of MC250/125

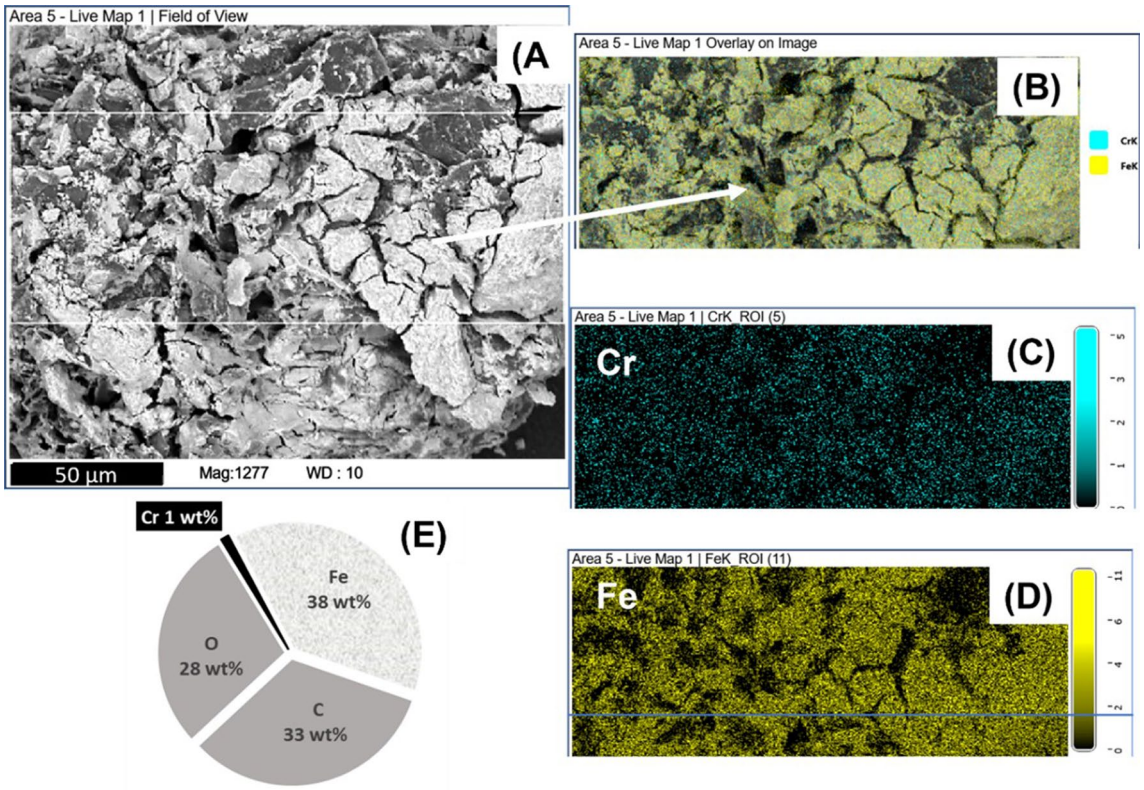

Fig. 5 EDAX of Sample 7–2—MC250/125 after 1020 min absorbing Cr(VI). **A** SEM micrograph; **B** Cr and Fe mapping in the centre area of **A**; **C** Cr mapping; **D** Fe mapping; and **E** semiquantitative percentage of the four elements encountered

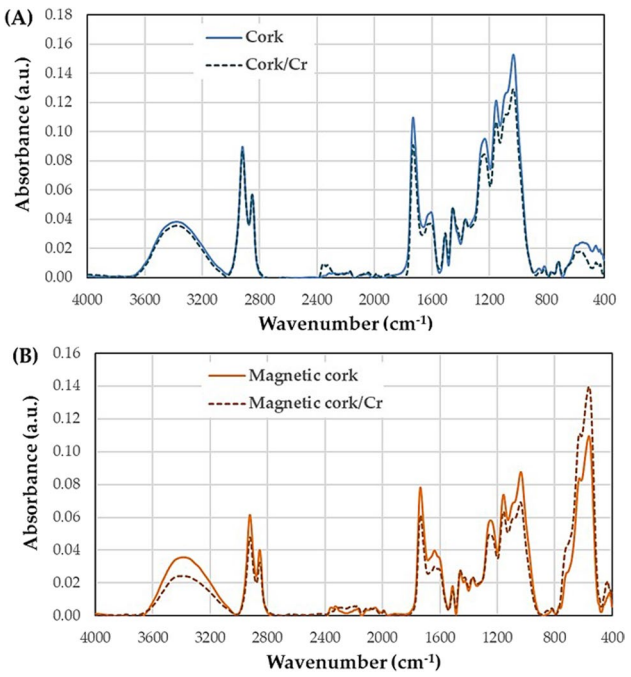

Fig. 6 FTIR spectra (**A**) natural cork before and after adsorbing chromium; (**B**) magnetic cork before and after adsorbing chromium

cork structure or skeleton from 1000 cm^{-1} to 1800 cm^{-1}. The peaks found in this area corresponded to the tension vibration and the stretching vibration of C–O at 1030 and 1154 cm^{-1}, respectively, and the bending and deformation vibration of C–H at 1255, 1367, and 1450 cm^{-1}. At 1507 cm^{-1}, the aromatic ring stretching vibration (C = C) was seen. The bending vibration of H–O–H was found at 1630 cm^{-1}, and at 1735 cm^{-1}, the stretching vibration of the carbonyl group (C = O). These peaks corresponded to aliphatic fatty esters. According to these peaks, G-lignin, carbohydrates, and lignin were cork constituents (Miranda et al. 2013). All those bands appeared in the four tested materials, with small differences among them. Thus, in Fig. 5A, for cork and cork after Cr(VI) adsorption, the peaks corresponding to the C–H and C = C bonds did not change, between the two corks. However, peaks corresponding to carbonyl and ester bonds decreased; therefore, Cr seemed to have bound to these groups. On the other hand, in Fig. 6B, all peaks decreased except those related to bending vibrations, which remained constant.

Furthermore, for the magnetic cork (Fig. 6B), below 800 cm^{-1}, there was an area that corresponded to Fe–O vibrations of magnetite (Fe_3O_4) at 425, 553, and 624 cm^{-1} (Bordbar et al. 2014), together with rocking vibration of $(CH_2)_n$ at 726 cm^{-1}. In the same area, the chromium peaks

corresponding to Cr_2O_3 at 610 and 545 cm^{-1} could be found (Madi et al. 2007). However, these chromium peaks were not observed at the spectrum due to their overlapping with iron peaks and the low concentration of chromium in relation to magnetite (Fig. 5B), although a slight increase in these bands can be seen for magnetic cork after adsorption of Cr(VI).

Considering these spectra, it would be possible to see if any groups oxidize due to the effect of chromium adsorption. This oxidize effect was observed by Sen et al. (Şen et al. 2012), with lignin playing an important role in the adsorption of Cr(VI) and its reduction to Cr(III). The groups that could be oxidized were the C-H groups, which would have provided a decrement of the double peak at 2850–2923 cm^{-1} and, consequently, an increment of the carbonyl or ester groups. However, this effect was not observed, perhaps due to the low chromium concentration and the high penetration of infrared radiation into the material.

XPS spectroscopy

XPS is the most adequate technique to know the surface composition, since the electrons only penetrate 10 nm, while 1 keV X-radiation can penetrate more than 1000 nm into a solid, and for FTIR-ATR, penetration depth is between 0.5 and 2 mm.

At acidic pH, Cr(VI) can be reduced to Cr(III) after contact with lignocellulosic materials, and the converted Cr(III) could be totally or partially released into the solution (Fiol et al. 2008; Park et al. 2008). Therefore, it is important to determine if the reduction of Cr(VI) took place when it was in contact with magnetic cork since it could not be seen by FTIR-ATR.

The elemental composition and surface chemical bonds of both natural and magnetic cork powder were analysed by XPS (Supplementary Fig. 8). Both samples presented two main bands assigned to C1s and O1s. Besides, magnetic cork displayed a small band of Fe2p, while after adsorption, a very small Cr2p band was observed.

Table 5 shows the atomic percentage of all elements on the surface, together with the percentages of each bond and their binding energy provided by the deconvolution of the main bands for the four cork types.

When the natural cork before and after adsorption was compared, an increase in the percentage of oxygen (8%) and a decrease in carbon (3%) were found, in addition to a small amount of chromium, which slightly increased the O/C ratio. This could be an indicator of the decrement of the C-H bonds and an increase in the C-O bonds. In the case of

Table 5 XPS analysis of elements on the surface of the four cork types (Benoit 2003)

	Elements and bond types	At.%				Binding energy (eV)						
		C	MC	C_Cr	MC_Cr	C	MC	C_Cr	MC_Cr	Average ± SD		
Survey scan	C	80.4	36.5	78.3	38.3							
	O	19.6	49.5	21.3	49.2							
	Fe		14.0		11.5							
	Cr			0.4	1.0							
	O/C	0.2	1.4	0.3	1.3							
C1s	C–C/C–H	61.0	52.7	63.7	49.0	284.6	284.6	284.6	284.6	284.6	±	0.0
	C-O	11.7	5.2	13.5	9.9	285.6	285.1	285.6	285.4	285.4	±	0.2
	C–O–C	22.7	29.4	19.1	28.5	286.4	286.3	286.6	286.3	286.4	±	0.1
	C = O	4.6	12.7	3.7	12.6	288.4	288.4	288.3	288.2	288.3	±	0.1
O1s	Fe_3O_4/Cr_2O_3		64.1		51.0		530.1		530.0	530.0	±	0.1
	O = C/$Cr(OH)_3$/FeOOH		16.6	16.1	29.7		531.4	531.6	531.3	531.4	±	0.2
	O–C = O	94.4	19.2	81.3	19.3	532.7	532.7	532.9	532.9	532.8	±	0.1
	O–C	5.6				533.7						
	O-Cr(VI)			2.6				534.4				
Fe2p	Fe(II)-O		14.8		15.6		710.1		710.0	710.0	±	0.1
	Fe_3O_4		62.9		63.5		711.1		711.1	711.1	±	0.0
	Fe(III)-O		17.5		15.7		713.5		713.6	713.6	±	0.1
	Shake-up		4.8		5.2		718.9		718.9	718.9	±	0.0
Cr2p	Cr			4.8				574.6				
	Cr_2O_3			47.6	63.7			576.2	576.3	576.2	±	0.1
	$Cr(OH)_3$			28.6	28.7			577.7	577.6	577.6	±	0.1
	Cr(VI)			19.0				579.6				

MC before and after Cr(VI) adsorption, it was found that after the adsorption, a slight increase in carbon (5%) was observed, maintaining oxygen and decreasing Fe. However, the Cr(VI) was 60% higher than in natural cork with Cr(VI). The ratio O/C for MC was higher than 1 because there was more oxygen than in natural cork.

XPS spectra for the C1s are shown in Supplementary Fig. 9 and Table 5. In all of them, four peaks were observed: C–C and C–H (284.6 eV), C–O (285.4), C–O–C (286.3 eV), and O–C = O (288.4 eV) (Roland Benoit CNRS Orléans; Moulder et al. 1993; Choudhary et al. 2017). Therefore, MC presented the same carbon bonds as C. Supplementary Fig. 9A corresponds to the natural cork powder without Cr(VI) (C) and Supplementary Fig. 9C with Cr(VI) (C_Cr). When they were compared, a decrement of 7% for oxidated bonds C–O was found.

Supplementary Fig. 9B (magnetic cork, MC) and 9D (magnetic cork with chromium, MC_Cr) shows a significant decrease in the peaks of the four types of links found in relation to natural cork. However, when the percentages of carbon bonds were considered, a decrement of 14% in the C–C bond and an increase of 18% in the C–O group were observed. Despite these differences, when MC before and after Cr (VI) adsorption was compared, the C–O oxidated bonds were a 7% higher in MC_Cr than in MC.

The deconvolution of the oxygen O1s band only presented two peaks for the natural cork (Supplementary Fig. 10 and Table 5), which corresponded to the O–C = O ester bond at 532.8 eV and the O–C bond at 533.7 eV (Supplementary Fig. 10A). The O–C groups disappeared for the other three studied samples. After Cr(VI) adsorption, the natural cork had three peaks at 531.4 eV, 532.8 eV, and 534.4 eV for bonds of carbonyl/hydroxyl groups (O = C/CrOH), O–C = O, and O–Cr(VI), respectively (Supplementary Fig. 10C). Thus, the ester group decreased by 14% in relation to the natural cork, but the carbonyl group increased by 16%. However, the hydroxyl peak with the Cr(III) could be found at the same energy (Moulder et al. 1993; Choudhary et al. 2017).

When the MC was analysed (Supplementary Fig. 10B and Table 5), magnetite was fundamentally found at 530 eV combined with Fe(III) oxyhydroxide (OH–Fe = O) and carbonyl (O = C) at 531.4 eV and ester bonds (O–C = O) at 532.8 eV (Fig. 10B). By adsorbing Cr(VI) (Supplementary Fig. 10D), both magnetite and Cr_2O_3 were at 530 eV, but this peak decreased by 20% in relation to MC. Furthermore, carbonyl bonds increased by 44%, but Fe(III) oxyhydroxide and Cr(III) hydroxyls could not be differentiated at 531.4 eV. However, the bond of the ester group remained constant.

According to ultraviolet spectra (Sect. "Materials") and XPS for the O1s band, Cr(VI) was adsorbed on the cork surface; thus, a reduction from Cr(VI) to Cr(III) occurred. This reduction seemed to be complete when using the magnetic cork, and a small amount remained in the case of natural cork. Logically, if Cr(VI) was reduced, some compounds needed to be oxidized. In theory, the formation of more carbonyl groups for natural and magnetic cork after Cr(VI) adsorption seemed sufficient to suggest that some cork groups, such as C-O, were oxidized.

XPS spectra of Fe2p did not change for the MC before and after Cr(VI) adsorption. Both of them presented magnetite at 711.1 eV and Fe (II and III) hydroxyl at 710 and 713.6 eV, respectively (Fig. 7A and B). Besides, both showed a satellite peak (shake-up) at 718.9 eV, resulting from the instrumental effect (Moulder et al. 1993). Satellite peaks were found at binding energy higher than characteristic peaks of the sample, with intensity and spacing characteristic given by the X-ray anode material. The spin–orbit splitting was 13.6 eV in both spectra.

XPS spectra revealed that chromium had different oxidation states when it was adsorbed by natural cork powder or magnetic cork. The percentages and bond types are shown in Fig. 8A for natural cork after the adsorption of Cr(VI), and the separation between 2p3/2 and 2p1/2 was 9.6 eV. Therefore, it was possible to identify metallic chromium at 574.6 eV, Cr(III) oxide (Cr_2O_3) at 576.2 eV, Cr(III) hydroxyl ($Cr(OH)_3$) at 577.6 eV, and a part of Cr(VI) as K_2CrO_4 (reactive used to prepare the original solution) at 579.6 eV. The same compounds were found by Sen et al. (Şen et al. 2012) when they removed Cr(IV) with natural cork. The O1s equivalent of these Cr2p is observed in Supplementary Fig. 10C.

The Cr(VI) reduction was complete when magnetic cork was used (Fig. 8B); Cr(III) oxide and hydroxyl were found in this case, at 576.2 and 577.6 eV, respectively, with a separation between Crp3/2 and Crp1/2 of 9.8 eV.

It was evident that both natural and magnetic corks were capable of reducing Cr(VI) to Cr(III) or metallic Cr. However, oxidation of cork groups was not observed; while the oxidation of C-H bonds was expected, the peak corresponding to the C–C and C–H bonds did not decrease between Supplementary Fig. 10A and C. Nevertheless, the peak of O–C disappeared, and more carbonyl groups were observed, while magnetite and Cr_2O_3 were found at the same binding energy. Consequently, it was not possible to determine how many bonds were O = C. For magnetic cork, no differences in these peaks were found when analysing Supplementary Fig. 110 and C, and Table 5. Choudhary et al. (Choudhary et al. 2017) found the oxidation of biochar groups (charcoal produced from plant matter) and Cr(VI) reduction. Chen et al. (Chen et al. 2018) investigated the effectiveness of activated carbon at acidic pH in reducing Cr(VI) to Cr(III), according to Eq. 12

$$Cr_2O_7^{2-} + R - C - H + H^+ \rightarrow Cr^{3+} + R - C = O/R - C - O \quad (12)$$

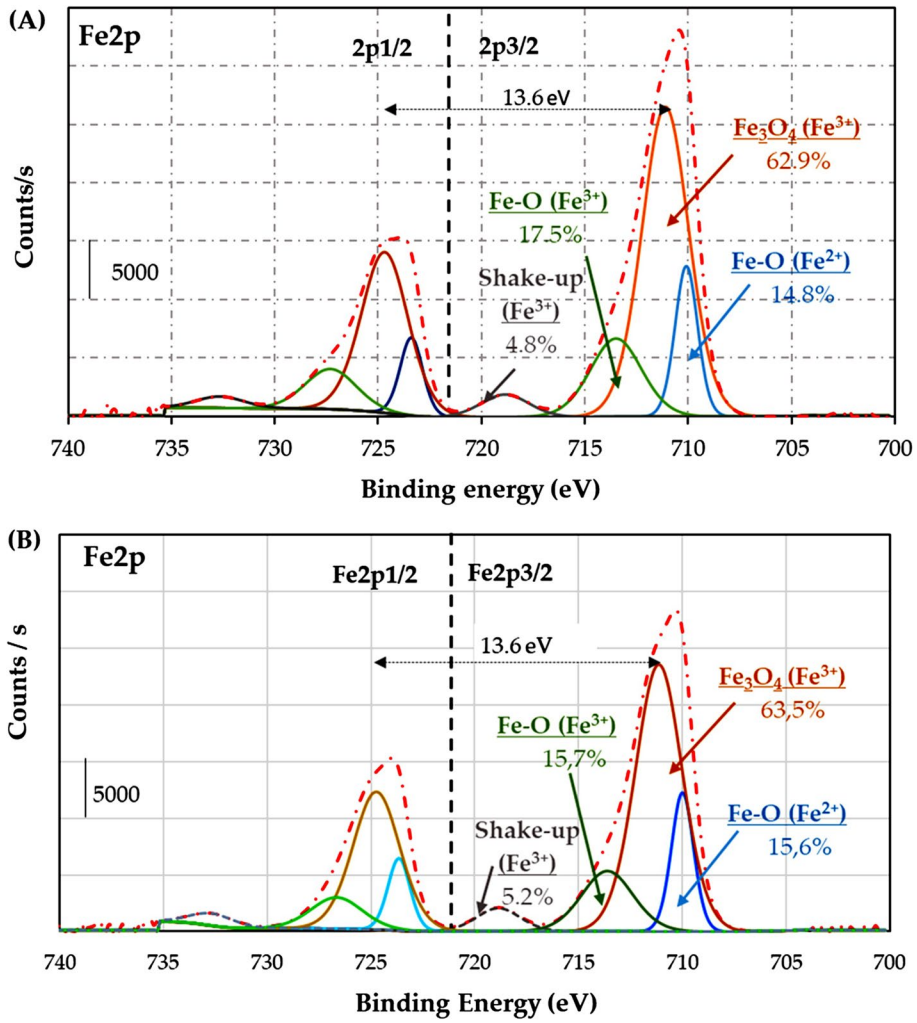

Fig. 7 XPS spectra of the Fe2p: **A** magnetic cork and **B** magnetic cork with chromium

Although the oxidation of cork was not definitively observed, it was evident that Cr(VI) was adsorbed and reduced to for Cr(III) species, such as Cr_2O_3 oxide and as hydroxide ($Cr(OH)_3$). The adsorption of Cr(VI) was facilitated by electrostatic attraction between anionic species and the protonated cork surface at pH = 4. The adsorption and reduction processes were mediated by the carbonyl and ester groups present on the cork surface. These interactions between Cr(VI) and magnetic cork or cork are in agreement with the Temkin isotherm model, where a good correlation was observed (Fig. 1b).

The oxidation of cork could be justified if the oxygen atoms from Cr(III) hydroxide and chromium(III) oxide were to bond with the carbonyl and ester groups, from which they are derived, thereby resulting in an increase in oxidized groups. This oxidation was also observed when the natural cork adsorbed magnetite, although it was not also possible to know the extent of this oxidation.

Conclusions

This work has demonstrated that magnetic cork, obtained by an easy and cost-effective co-precipitation method, can effectively be used to treat wastewater to remove hexavalent chromium. One of the main advantages magnetic cork offers compared to natural cork is its ease of removal from aqueous solutions.

The Langmuir and Temkin isotherm models were able to explain the adsorption process, with uniform active adsorption sites, molecule's ability to bind to the surface, monolayer formation, uniform distribution of binding energy, and interactions between the adsorbate and the adsorbed species. Through absorbance measurements, it was found that smaller particles exhibit higher efficiency in terms of adsorbent capacity compared to larger particles. Besides, the adsorption process can be adequately

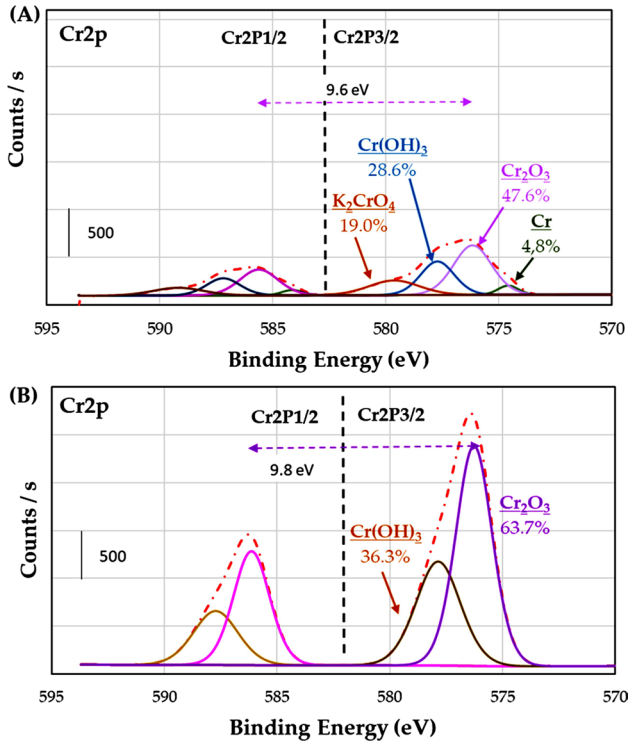

Fig. 8 XPS spectra of the Cr2p: **A** cork with chromium and **B** magnetic cork with chromium

described by a pseudo-second-order kinetic model. Additionally, hexavalent chromium is reduced to its Cr(III) and Cr(0) species. While FTIR and XPS confirmed the reduction of hexavalent chromium, the specific reducing species were not identified using these techniques.

From a thermodynamic standpoint, the reactions are endothermic and spontaneous. Among them, the adsorption reaction with the highest absolute value of $\Delta G°$ is attributed to MC53/38, making it the most favoured material with the highest Cr(IV) adsorbance. MC53/38 effectively removes 99% of a 100 mg/L Cr(VI) solution within two hours at 50 °C.

Therefore, in this work, the efficacy of using magnetic cork with a particle size of 53/38 µm as an adsorbent for hexavalent chromium is demonstrated, integrating various extraction methods (magnetic, bio-adsorbent, and electrochemical reduction adsorption techniques) while reusing industrial wastes. Besides, a potentially effective strategy for managing the end-of-life phase of these materials could be their use as anodes in potassium-ion batteries.

Supplementary Information The online version contains supplementary material available at https://doi.org/10.1007/s13201-024-02322-z.

Author contribution J.A. performed conceptualization, methodology, formal analysis, investigation, resources, writing—original, writing—review—editing. S.L. involved in investigation, writing—review—editing. J.C.R. took part in supervision, funding acquisition. M.A.M. involved in formal analysis, supervision, funding acquisition.

Funding No external funding.

Declarations

Conflict of interest The authors declare no conflict of interest.

References

Abenojar J, Barbosa AQ, Ballesteros Y et al (2014) Effect of surface treatments on natural cork: surface energy, adhesion, and acoustic insulation. Wood Sci Technol 48:207–224. https://doi.org/10.1007/s00226-013-0599-7

Abenojar J, López de Armentia S, Barbosa AQ et al (2020) Coating cork particles with iron oxide: effect on magnetic properties. Wood Sci Technol 54:869–889. https://doi.org/10.1007/s00226-020-01191-4

Ahmad R, Hasan I (2017) Efficient Remediation of an Aquatic Environment Contaminated by Cr(VI) and 2,4-Dinitrophenol by XG-g-Polyaniline@ZnO Nanocomposite. J Chem Eng Data 62:1594–1607. https://doi.org/10.1021/acs.jced.6b00963

Ahmad R, Hasan I, Mittal A (2017) Adsorption of Cr (VI) and Cd (II) on chitosan grafted polyaniline-OMMT nanocomposite: Isotherms, kinetics and thermodynamics studies. Desalination Water Treat 58:144–153. https://doi.org/10.5004/dwt.2017.0414

Bordbar AK, Rastegari AA, Amiri R et al (2014) Characterization of Modified Magnetite Nanoparticles for Albumin Immobilization. Biotechnol Res Int 2014:1–6. https://doi.org/10.1155/2014/705068

Cai Y, Wu Y, Yang L et al (2022) A wood sponge sensor for heavy metal ion detection and adsorption. Wood Sci Technol 56:1175–1190. https://doi.org/10.1007/s00226-022-01390-1

Chen Y, An D, Sun S et al (2018) Reduction and removal of chromium VI in water by powdered activated carbon. Materials 11:269. https://doi.org/10.3390/ma11020269

Choudhary B, Paul D, Singh A, Gupta T (2017) Removal of hexavalent chromium upon interaction with biochar under acidic conditions: mechanistic insights and application. Environ Sci Pollut Res 24:16786–16797. https://doi.org/10.1007/s11356-017-9322-9

Das DD, Mahapatra R, Pradhan J et al (2000) Removal of Cr(VI) from aqueous solution using activated cow dung carbon. J Colloid Interface Sci 232:235–240. https://doi.org/10.1006/jcis.2000.7141

Fiol N, Escudero C, Villaescusa I (2008) Chromium sorption and Cr(VI) reduction to Cr(III) by grape stalks and yohimbe bark.

Bioresour Technol 99:5030–5036. https://doi.org/10.1016/j.biortech.2007.09.007
Freundlich HMF (1906) Over the adsorption in solution. J Phys Chem 57:385–471
Guleria A, Kumari G, Lima EC et al (2022) Removal of inorganic toxic contaminants from wastewater using sustainable biomass: a review. Sci Total Environ 823:153689. https://doi.org/10.1016/j.scitotenv.2022.153689
Gupta VK, Rastogi A (2008) Sorption and desorption studies of chromium(VI) from nonviable cyanobacterium Nostoc muscorum biomass. J Hazard Mater 154:347–354. https://doi.org/10.1016/j.jhazmat.2007.10.032
Gupta A, Sharma V, Sharma K et al (2021) A review of adsorbents for heavy metal decontamination: growing approach to wastewater treatment. Materials 14:4702. https://doi.org/10.3390/ma14164702
Hinz C (2001) Description of sorption data with isotherm equations. Geoderma 99:225–243
Ho YS, Mckay G (1999) Pseudo-second order model for sorption processes. Process Biochem 34:451–465
Hu J, Chen G, Lo IMC (2005) Removal and recovery of Cr(VI) from wastewater by maghemite nanoparticles. Water Res 39:4528–4536. https://doi.org/10.1016/j.watres.2005.05.051
Karnib M, Kabbani A, Holail H, Olama Z (2014) Heavy metals removal using activated carbon, silica and silica activated carbon composite. Energy Procedia 50:113–120. https://doi.org/10.1016/j.egypro.2014.06.014
Kooh MRR, Dahri MK, Lim LBL (2017) Removal of methyl violet 2B dye from aqueous solution using Nepenthes rafflesiana pitcher and leaves. Appl Water Sci 7:3859–3868. https://doi.org/10.1007/s13201-017-0537-1
Kooh MRR, Dahri MK, Lim LBL et al (2018) Separation of acid blue 25 from aqueous solution using water lettuce and agro-wastes by batch adsorption studies. Appl Water Sci 8:61. https://doi.org/10.1007/s13201-018-0714-x
Kumar H, Maurya KL, Gehlaut AK et al (2020) Adsorptive removal of chromium(VI) from aqueous solution using binary bio-polymeric beads made from bagasse. Appl Water Sci 10:21. https://doi.org/10.1007/s13201-019-1101-y
Lagergren S (1898) About the theory of so-called adsorption of soluble substances. Kungliga Svenska Vetenskapsakademiens Handlingar 24:1–39
Langmuir I (1916) The constitution and fundamental properties of solids and liquids. J Am Chem Soc 38:22212295. https://doi.org/10.1021/ja02268a002
Lata S, Singh PK, Samadder SR (2015) Regeneration of adsorbents and recovery of heavy metals: a review. Int J Environ Sci Technol 12:1461–1478. https://doi.org/10.1007/s13762-014-0714-9
Ma J, Liu C (2021) Turning waste into treasure: Reuse of contaminant-laden adsorbents (Cr(VI)-Fe3O4/C) as anodes with high potassium-storage capacity. J Colloid Interface Sci 582:1107–1115. https://doi.org/10.1016/j.jcis.2020.08.110
Madi C, Tabbal M, Christidis T et al (2007) Microstructural characterization of chromium oxide thin films grown by remote plasma assisted pulsed laser deposition. J Phys Conf Ser 59:600–604. https://doi.org/10.1088/1742-6596/59/1/128
Miao M, Lu Q, Wang X et al (2023) Removal of micro-organic contaminants from wastewater: a critical review of treatment technology. Next Mater 1:100016. https://doi.org/10.1016/j.nxmate.2023.100016
Miranda I, Gominho J, Pereira H (2013) Cellular structure and chemical composition of cork from the Chinese cork oak (*Quercus variabilis*). J Wood Sci 59:1–9. https://doi.org/10.1007/s10086-012-1300-8
Mittal A, Ahmad R, Hasan I (2016) Iron oxide-impregnated dextrin nanocomposite: synthesis and its application for the biosorption of Cr(VI) ions from aqueous solution. Desalination Water Treat 57:15133–15145. https://doi.org/10.1080/19443994.2015.1070764
Mohamed Khalith SB, Rishabb Anirud R, Ramalingam R et al (2021) Synthesis and characterization of magnetite carbon nanocomposite from agro waste as chromium adsorbent for effluent treatment. Environ Res 202:111669. https://doi.org/10.1016/j.envres.2021.111669
Mohammadi SA, Najafi H, Zolgharnian S et al (2022) Biological oxidation methods for the removal of organic and inorganic contaminants from wastewater: a comprehensive review. Sci Total Environ 843:157026. https://doi.org/10.1016/j.scitotenv.2022.157026
Mohammadkhani F, Montazer M, Latifi M (2019) Microwave absorption characterization and wettability of magnetic nano iron oxide/recycled PET nanofibers web. J Text Inst 110:989–999. https://doi.org/10.1080/00405000.2018.1559908
Mohan D, Pittman CU (2006) Activated carbons and low cost adsorbents for remediation of tri- and hexavalent chromium from water. J Hazard Mater 137:762–811. https://doi.org/10.1016/j.jhazmat.2006.06.060
Pantsar-Kallio M, Manninen PKG (1996) Speciation of chromium in waste waters by coupled column ion chromatography-inductively coupled plasma mass spectrometry. J Chromatogr A 750:89–95
Park D, Ahn CK, Kim YM et al (2008) Enhanced abiotic reduction of Cr(VI) in a soil slurry system by natural biomaterial addition. J Hazard Mater 160:422–427. https://doi.org/10.1016/j.jhazmat.2008.03.044
Pesqueira JFJR, Pereira MFR, Silva AMT (2020) Environmental impact assessment of advanced urban wastewater treatment technologies for the removal of priority substances and contaminants of emerging concern: a review. J Clean Prod 261:121078. https://doi.org/10.1016/j.jclepro.2020.121078
Qasem NAA, Mohammed RH, Lawal DU (2021) Removal of heavy metal ions from wastewater: a comprehensive and critical review. NPJ Clean Water 4:36. https://doi.org/10.1038/s41545-021-00127-0
Sanz-Santos E, Álvarez-Torrellas S, Ceballos L et al (2021) Application of sludge-based activated carbons for the effective adsorption of neonicotinoid pesticides. Appl Sci 11:3087. https://doi.org/10.3390/app11073087
Şen A, Àngels Olivella M, Fiol N et al (2012) Removal of chromium (VI) in aqueous environments using cork and heat-treated cork samples from Quercus Cerris and Quercus Suber. BioResources 7:4843–4857
Sfaksi Z, Azzouz N, Abdelwahab A (2011) Use of cork waste as biosorbent for hexavalent chromium. Adv Mater Res 324:497–500. https://doi.org/10.4028/www.scientific.net/AMR.324.497
Song W, Gao B, Zhang T et al (2015) High-capacity adsorption of dissolved hexavalent chromium using amine-functionalized magnetic corn stalk composites. Bioresour Technol 190:550–557. https://doi.org/10.1016/j.biortech.2015.01.103
Spaltro A, Pila M, Simonetti S et al (2018) Adsorption and removal of phenoxy acetic herbicides from water by using commercial activated carbons: experimental and computational studies. J Contam Hydrol 218:84–93. https://doi.org/10.1016/j.jconhyd.2018.10.003
Sudha Bai R, Abraham TE (2003) Studies on chromium(VI) adsorption-desorption using immobilized fungal biomass. Bioresour Technol 87:17–26
Todescato D, Mayer DA, Cechinel MAP et al (2021) Cork granules as electron donor in integrated reduction/oxidation and sorption processes for hexavalent chromium removal from synthetic aqueous solution. J Environ Chem Eng 9:105001. https://doi.org/10.1016/j.jece.2020.105001
Velempini T, Ahamed MEH, Pillay K (2023) Heavy-metal spent adsorbents reuse in catalytic, energy and forensic applications- a new approach in reducing secondary pollution associated with

adsorption. Results Chem 5:100901. https://doi.org/10.1016/j.rechem.2023.100901
Verma R, Maji PK, Sarkar S (2023) Removal of hexavalent chromium from impaired water: Polyethylenimine-based sorbents—A review. J Environ Chem Eng 11:109598. https://doi.org/10.1016/j.jece.2023.109598
Walter J, Weber J, ASCE A, Morris JC (1963) Kinetics of Adsorption on Carbon from Solution. J Sanit Eng Div 89(2):31–59
Wang S, Wang K, Dai C et al (2015) Adsorption of Pb2+ on amino-functionalized core-shell magnetic mesoporous SBA-15 silica composite. Chem Eng J 262:897–903. https://doi.org/10.1016/j.cej.2014.10.035
Wang CC, Du XD, Li J et al (2016) Photocatalytic Cr(VI) reduction in metal-organic frameworks: a mini-review. Appl Catal B 193:198–216. https://doi.org/10.1016/j.apcatb.2016.04.030
Wang Q, Lai Z, Mu J et al (2020) Converting industrial waste cork to biochar as Cu (II) adsorbent via slow pyrolysis. Waste Manage 105:102–109. https://doi.org/10.1016/j.wasman.2020.01.041
Xu P, Zeng GM, Huang DL et al (2012) Use of iron oxide nanomaterials in wastewater treatment: a review. Sci Total Environ 424:1–10. https://doi.org/10.1016/j.scitotenv.2012.02.023
Xu J, Zhou L, Jia Y et al (2015) Adsorption of thorium (IV) ions from aqueous solution by magnetic chitosan resins modified with triethylene-tetramine. J Radioanal Nucl Chem 303:347–356. https://doi.org/10.1007/s10967-014-3227-6
Yang J, Fu M, Tan M et al (2020) Photocatalytic Reduction of Cr(VI) on a 3.0% Au/Sr0.70Ce0.20WO4 Photocatalyst. ACS Omega 5:26755–26762. https://doi.org/10.1021/acsomega.0c03743
Zanin E, Scapinello J, de Oliveira M et al (2017) Adsorption of heavy metals from wastewater graphic industry using clinoptilolite zeolite as adsorbent. Process Saf Environ Prot 105:194–200. https://doi.org/10.1016/j.psep.2016.11.008
Zelmanov G, Semiat R (2011) Iron (Fe+3) oxide/hydroxide nanoparticles-based agglomerates suspension as adsorbent for chromium (Cr+6) removal from water and recovery. Sep Purif Technol 80:330–337. https://doi.org/10.1016/j.seppur.2011.05.016
American public health association, American water works association, water environment federation (2012) standard methods for the examination of water and wastewater, 22nd edn.
Constales D, Yablonsky GS, D'hooge DR, et al (2017a) Chapter 5. Thermodynamics. In: Advanced Data Analysis and Modelling in Chemical Engineering. Elsevier, pp 159–220
Constales D, Yablonsky GS, D'hooge DR, et al (2017b) Chapter 3—complex reactions: kinetics and mechanisms—ordinary differential equations—graph theory. In: advanced data analysis and modelling in chemical engineering. Elsevier, pp 35–82
Giles CH, MacEwan TH, Nakhwa SN, Smith D (1960) Studies in adsorption. Part XI. A system of classification of solution adsorption isotherms, and its use in diagnosis of adsorption mechanisms and in measurement of specific surface areas of solids. J Chem Soc 3973–3993
Herrera GMD, Ordoñez APP, Anaguano AH (2013) Standardization of diphenylcarbazid as an indicator and a complexity factor in the identification of chromium hexavalent—Cr (VI). Producción + Limpia 8:9–20
Hlavinek P, Winkler I, Marsalek J, Mahrikova I (2011) Advanced Water Supply and Wastewater Treatment: A Road to Safer Society and Environment. NATO Science for Peace and Security Series C: Environmental Security. https://doi.org/10.1007/978-94-007-0280-6
Kerur SS, Bandekar S, Hanagadakar MS, et al (2020) Removal of hexavalent Chromium-Industry treated water and Wastewater: a review. In: Materials Today: Proceedings. Elsevier Ltd pp 1112–1121
Mahajan T, Paikaray S, Mahajan P (2023) Applicability of the equilibrium adsorption isotherms and the statistical tools on to them: a case study for the adsorption of fluoride onto Mg-Fe-CO3LDH. In: Journal of Physics: Conference Series. Institute of Physics
Moulder JF, Stickle WF, Sobol PE', et al (1993) Handbook of X-ray Photoelectron Spectroscopy. Perkin-Elmer Corporation
Benoit R, (2003) XPS, AES, UPS and ESCA. lasurface.com. http://www.lasurface.com (Accessed on 22 May 2023)
World Health Organization (2017) Guidelines for Drinking-water Quality, Fourth Edition